View metadata, citation and similar papers at core.ac.uk
brought to you by CORE
provided by Archivio istituzionale della ricerca - Università di Palermo

Phys Chem Minerals (2015) 42:347–362
DOI 10.1007/s00269-014-0725-6

ORIGINAL PAPER

Modelling of thermo-chemical properties over the sub-solidus MgO–FeO binary, as a function of iron spin configuration, composition and temperature

Marcello Merli · Luciana Sciascia · Alessandro Pavese · Valeria Diella

Received: 8 July 2014 / Accepted: 23 November 2014 / Published online: 10 December 2014
© Springer-Verlag Berlin Heidelberg 2014

Abstract Thermo-chemical properties and *T*–*X* phase relations diagram of the (Mg,Fe)O solid solution are modelled using mixing Helmholtz energy, $\Delta F(T,x)_{\text{mixing}}$, calculated by quantum mechanical and semi-empirical techniques. The sub-solidus MgO–FeO binary has been explored as a function of composition, with iron either in high-spin (HS) or low-spin (LS) configuration. Only the HS model provides physically sound results at room pressure, yielding a correct trend of cell edge versus composition, whereas LS's issues are at variance with observations. Mixing Helmholtz energy has been parametrized by the following relationship: $\Delta F(T,x)_{\text{mixing}} = x \times y \times [U_0(T) + U_1(T) \times (x - y) + U_2(T) \times (x - y)^2] - T \times S(x,y)_{\text{config}}$, where $y = 1-x$ and $U_j(T)$ are polynomials in T of the second order. $\Delta F(T,x)_{\text{mixing}}$ exhibits a quasi-symmetric behaviour and allows one to build the *T*–*X* phase relations diagram over the MgO–FeO join. The HS model including vibrational contribution to the Helmholtz energy predicts a solid solution's critical temperature of some 950 K, remarkably larger than olivine's and Mg–Fe garnet's. All this points to a more difficult Mg–Fe mixing in periclase-like structure than olivine and garnet, which, in turn, provide more structure degrees of freedom for atomic relaxation. From $\Delta F(T,x)_{\text{mixing}}$, we have then derived $\Delta H(T,x)_{\text{excess}}$ and $\Delta S(T,x)_{\text{excess}}$. The former, characterized by a quasi-regular behaviour, has been parametrized through $W \times x \times (1-x)$, obtaining $W_{\text{H,Mg–Fe}}$ of 17.7(5) kJ/mol. $\Delta S(T,x)_{\text{excess}}$, in turn, increases as a function of temperature, showing absolute figures confined within 0.1 J/mol/K. Mixing Gibbs energy, calculated combining the present issues with earlier theoretical determinations of the magnesio-wüstite's elastic properties, has shown that the HS configuration is stable and promote Mg–Fe solid solution up to ≈15 GPa.

Keywords Mixing energy · Ab initio and semi-empirical modelling · (Mg,Fe)O

Introduction

The Mg–Fe mixing is a complex phenomenon, important to form solid phases that participate in many a natural process over a wide pressure–temperature (*P*–*T*) range. The sub-solidus MgO–FeO binary has motivated a relevant interest as magnesium-wüstite solid solution, (Mg,Fe)O with periclase-like crystal structure (Fm-3m), and is a major mineral constituent of the lower mantle of the Earth, along with $(Mg,Fe)SiO_3$ perovskite, and of other terrestrial planets of the Solar System, as deduced by geochemical and mineralogical studies of meteorites (Jeanloz and Knittle 1989; Lee et al. 2004; Jeanloz and Lay 1993; Righter et al. 2006). Remarkable efforts have been steered to the study of MgO

Electronic supplementary material The online version of this article (doi:10.1007/s00269-014-0725-6) contains supplementary material, which is available to authorized users.

M. Merli · L. Sciascia
Dipartimento di Chimica e Fisica della Terra e Applicazioni alle Georisorse e ai Rischi Naturali, Università degli Studi di Palermo, Via Archirafi 36, 90123 Palermo, Italy
e-mail: marcello.merli@unipa.it

L. Sciascia
e-mail: luciana.sciascia@unipa.it

A. Pavese (✉)
Dipartimento Scienze della Terra "A. Desio", Università degli Studi di Milano, Via Botticelli 23, 20133 Milan, Italy
e-mail: alessandro.pavese@unimi.it

A. Pavese · V. Diella
National Reseach Council (CNR), IDPA, Section of Milan, Via Botticelli 23, 20133 Milan, Italy

and FeO at such a *P*–*T* regime as is representative of the interiors of the Earth (Duffy et al. 1995; Karki et al. 1997; Fischer et al. 2011; Mao et al. 1996; Fang et al. 1998; Jeanloz and Ahrens 1980; Yagi et al. 1985, 1988; Fei and Mao 1994). An increase of pressure on (Mg,Fe)O could lead to a gradual ex-solution from the rock salt phase (McCammon et al. 1983; Duffy et al. 1995; Dubrovinsky et al. 2000) into magnesium-rich and iron-rich oxide components, with relevant bearings to the formation of the mantle heterogeneity (van der Hilst et al. 1997; Garnero 2000). A further complexity is added by that the (Mg,Fe)O solid solution's properties, Fe spin states and high-to-low spin transition triggered by *P* are strictly related to each other (see, for instance: Jacobsen et al. 2002; Kondo et al. 2004; Speziale et al. 2005; Kantor et al. 2006; Persson et al. 2006; Goncharov et al. 2006; Yoshiasa et al. 2009; Crowhurst et al. 2008; Lyubutin et al. 2009; Lin et al. 2013). Besides, the spin-switch affects the partitioning of Fe between (Mg,Fe)SiO_3 and (Mg,Fe)O with depth, and such an effect may (Cohen et al. 1997; Badro et al. 2003) or may not (Irifune et al. 2010) result in a stratified lower mantle and change elastic moduli, compressibility, radiative thermal conductivity, electrical transport, sound velocities and other physical–chemical properties of Fe–Mg-bearing minerals (Lin et al. 2009, Pasternak et al. 1997; Badro et al. 1999; Crowhurst et al. 2008; Antonangeli et al. 2011; Mao et al. 1996). Beside the role played by (Mg,Fe)O solid solution as a phase of the Earth mantle, magnesio-wüstite is also an accessory phase of reducing-condition contact metamorphism involving high-temperature reactions in which carbonatites undergo transformations (Wallmach et al. 1989; Cook and Bowman 2000; Wenzel et al. 2002; Müller et al. 2009; Ganino et al. 2013). The partitioning of Fe^{2+}–Mg between ferromagnetic mineral phases is then relevant to geo-thermometry at large, and, in such a context, attention has been paid to (Mg,Fe)O as a means to infer information about the activity–composition relations of olivine solid solutions (O'Neill et al. 2003; Sreçec et al. 1987). In addition to all this, (Mg,Fe)O solid solution exhibits a high-temperature behaviour that makes it of interest to technological aims, such as those meant to ceramics, steel production and ionic-conductivity (Bennet and Kwong 2010; Kwong et al. 2009; Smolin and Schmalzried 2003).

In view of the magnesio-wüstite's wide geological and technological scope, it is important to achieve as full an understanding as possible of the principles underlying the stability of the (Mg,Fe)O solid solution, as a function of those aspects that primarily affect its reactivity in the variety of the transformations in which it participates. In particular, modelling (Mg,Fe)O's thermo-chemical properties and *T*–*X* phase relations diagram as a function of composition and iron spin configuration represents a step to help interpreting both high-temperature and high-pressure–high-temperature natural reactions. In general, one has to take into account that for complex assemblages of interest to geologic processes the Gibbs energy of a phase is calculated as

$$G(P,T) = G(P_0,T_0) + \int_{P_0T_0}^{P_0T} \mathrm{d}G(P_0,T') + \int_{P_0T}^{PT} \mathrm{d}G(P',T), \tag{1}$$

where: P_0 and T_0 are reference pressure and temperature values (conventionally room conditions); and $G(P_0,T_0)$ is the Gibbs energy at P_0 and T_0, or the formation energy with respect to elements, or oxides. Hence, $G(P,T)$ is computed by two path integrals (Pavese and Diella 2007), the first of which is a P_0-isobaric from T_0 to T and requires a detailed knowledge of the energetics of a system at P_0 as a function of temperature.

Quantum mechanical and semi-empirical calculations, in combination with lattice dynamics and statistical thermodynamics, have proven a powerful tool to model the energetics of solid solutions (for instance: Vinograd et al. 2013, and references therein; De La Pierre et al. 2013; Scanavino and Prencipe 2013; Haider et al. 2012; Ruiz-Hernandez et al. 2010; Meyer et al. 2009. See for fundamentals of the Virtual Crystal Approximation: Bellaiche and Vanderbilt 2000. See for an introductory presentation to the double defect method: Vinograd and Winkler 2010).

In the light of the discussion above, we have decided to undertake the present work, in which we model thermochemical properties and *T*–*X* phase relations diagram as a function of iron spin configuration (low spin, $S = 0$: diamagnetic, LS; high spin, $S = 2$: antiferromagnetic/paramagnetic, HS), composition and temperature of (Mg,Fe)O. We aim to contribute to shed light on the magnesium-wüstite solid solution's mechanisms of stability and to provide a parametrization of the Helmholtz free energy as a function of *T* and *X* for practical uses. HS and LS iron states are here not mixed with one another, so that we treat Fe either in low or high-spin state, only. To our knowledge, the thermo-chemistry of the (Mg,Fe)O solid solution at room pressure and high temperature is still suffering from a general dearth of data, though its relevancy.

The present work is organized as follows: (1) calculation of energy (lattice energy by a hybrid approach based on Hartree–Fock and DFT; vibration energy by semi-empirical modelling) for a significant number of non-equivalent atomic Mg/Fe configurations and related compositions of magnesium-wüstite; (2) extraction of the parameters of a cluster expansion-type model and determination thereby of the partition function for different Mg/Fe compositions ($Z_{Mg–Fe}$); and (3) calculation of the Helmholtz free energy and parametrization as a function of *T* and *X*; determination of the *T*–*X* phase relations diagram for the (Mg,Fe)O

solid solution. As a by-product, we investigate the effects of pressure on the MgO–FeO binary's stability at high temperature exploiting earlier studies on elastic properties of (Mg,Fe)O.

Theoretical

Cluster expansion and solid solutions

We remind here some fundamentals for a cluster expansion-type approach to describe the energetics of solid solutions, using the discrete Chebyshev polynomials method (Sanchez et al. 1984). Let us represent by $\alpha(j)$ a variable defining the chemical content of the tenant of the jth site in a crystal solid solution, and assume that α can take $(2m + 1)$ values, i.e. –m, …, −1, (0), 1,…m. In general, an observable, A, is a function of the site occupancy configuration, hereafter $\{\alpha\}$, so that $A(\{\alpha\}) = A(\alpha\ (1),\ldots,\ \alpha(S))$, where S is the number of sites involved. Expanding in the canonical way the discrete $A(\{\alpha\})$ function as a series of discrete Chebyshev polynomials (Barnard et al. 1998) for each site, i.e. $\xi_{j(k)}(\alpha(k))$ where $j(k)$ is the polynomial order referred to the kth site and ranges from 0 to $(2m + 1)$, one obtains:

$$A(\{\alpha\}) = \Sigma_{k(1),\ldots,k(S)}\Phi_{k(1),k(2),\ldots,k(M)} \times [\xi_{k(1)}(\alpha(1)) \times \xi_{k(2)}(\alpha(2)) \times \cdots \times \xi_{k(S)}(\alpha(S))] \quad (2)$$

The terms of the series above can be rearranged as follows

$$A(\{\alpha\}) = {}^0A(\{\alpha\}) + {}^1A(\{\alpha\}) + {}^{11}A(\{\alpha\}) + {}^2A(\{\alpha\}) + {}^{111}A(\{\alpha\}) + {}^3A(\{\alpha\}) + \cdots,$$

where

$${}^0A(\{\alpha\}) = \{{}^0\Phi_{0(1),0(2),\ldots,0(S)} \times [\xi_{0(1)}(\alpha(1)) \times \xi_{0(2)}(\alpha(2)) \times \cdots \times \xi_{0(S)}(\alpha(S))]\}$$

$${}^1A(\{\alpha\}) = \{{}^1\Phi_{1(1),0(2),\ldots,0(S)} \times [\xi_{1(1)}(\alpha(1)) \times \xi_{0(2)}(\alpha(2)) \times \cdots \times \xi_{0(S)}(\alpha(S))] + \cdots + {}^1\Phi_{0(1),\ldots 1(L),\ldots,0(S)} \times [\xi_{0(1)}(\alpha(1)) \times \cdots \xi_{1(L)}(\alpha(L)) \times \cdots \times \xi_{0(S)}(\alpha(S))] + \cdots\}$$

$${}^{11}A(\{\alpha\}) = \{{}^{11}\Phi_{1(1),1(2),\ldots,0(S)} \times [\xi_{1(1)}(\alpha(1)) \times \xi_{1(2)}(\alpha(2)) \times \cdots \times \xi_{0(S)}(\alpha(S)] + \cdots + {}^{11}\Phi_{0(1),\ldots,1(L),\ldots,1(I),\ldots,0(S)} \times [\xi_{0(1)}(\alpha(1)) \times \cdots \xi_{1(L)}(\alpha(2)) \times \cdots \times \xi_{1(I)}(\alpha(I) \cdots \times \xi_{1(I)}(\alpha(S)] + \cdots\}$$

$${}^2A(\{\alpha\}) = \{{}^2\Phi_{2(1),0(2),\ldots,0(S)} \times [\xi_{2(1)}(\alpha(1)) \times \xi_{0(2)}(\alpha(2)) \times \cdots \times \xi_{0(S)}(\alpha(S))] + \cdots + {}^1\Phi_{0(1),0(2),\ldots,2(S)} \times [\xi_{0(1)}(\alpha(1)) \times \xi_{0(2)}(\alpha(2)) \times \cdots \times \xi_{2(S)}(\alpha(S))] + \cdots\}$$

$${}^{111}A(\{\alpha\}) = \{{}^{111}\Phi_{1(1),1(2),\ldots,0(S)} \times [\xi_{1(1)}(\alpha(1)) \times \xi_{1(2)}(\alpha(2)) \times \xi_{1(3)}(\alpha(3)) \times \cdots \times \xi_{0(S)}(\alpha(S)] + \cdots + {}^{111}\Phi_{0(1),\ldots,1(L),\ldots,1(H),\ldots,1(I),\ldots,0(S)} \times [\xi_{0(1)}(\alpha(1)) \times \cdots \xi_{1(L)}(\alpha(2)) \times \cdots \xi_{1(H)}(\alpha(2)) \times \cdots \xi_{1(I)}(\alpha(2)) \times \cdots \times \xi_{0(S)}(\alpha(S)] + \cdots\} \quad (3)$$

where ${}^{lpq\cdots}\Phi_{k(1)\ldots k(S)}$ is the coefficient of $[\xi_{k(1)}(\alpha(1)) \times \xi_{k(2)}(\alpha(2)) \times \cdots \times \xi_{k(S)}(\alpha(S))]$, i.e. the term of $l + p + q + \cdots$ order, assuming $0 < l \leq p\ldots$ and such that l, p… indicate polynomial orders other than zero. ${}^{lpq\cdots}A(\{\alpha\})$, in turn, is the corresponding contribution to the A observable; ${}^{11}A(\{\alpha\})$, for instance, represents the contribution due to all configurations which involve two sites described by discrete Chebyshev polynomials of degree one, i.e. two-atom clusters of total degree two, whereas for the other S-2 sites polynomial expansions of 0-order are used. For each ${}^{lpq\cdots}A(\{\alpha\})$ term, we gather the addends sharing the same $[\xi_{k(1)}(\alpha(1)) \times \xi_{k(2)}(\alpha(2)) \times \cdots \times \xi_{k(S)}(\alpha(S))]$ value in sets, which are then partitioned as a function of n-atom clusters, $\Omega(n)$, defined by a threshold distance, $r[\Omega(n)]$, between the involved atoms. In so doing, one can rewrite the summations above as follows:

$${}^0A(\{\alpha\}) = {}^0A$$

$${}^1A(\{\alpha\}) = \Sigma_\alpha^1 C_\alpha \times [\xi_1(\alpha)] \times {}^1n_\alpha = \Sigma_\alpha^1 A_\alpha \times {}^1n_\alpha$$

$${}^{11}A(\{\alpha\}) = \Sigma_{\alpha,\beta}\Sigma_{\Omega(2)}^{11} C_{\alpha\beta,\Omega(2)} \times [\xi_1(\alpha) \times \xi_1(\beta)] \times {}^{11}n_{\alpha\beta,\Omega(2)} = \Sigma_{\alpha<\beta}\Sigma_{\Omega)(2)}^{11} A_{\alpha\beta,\Omega(2)} \times {}^{11}n_{\alpha\beta,\Omega(2)}$$

$${}^2A(\{\alpha\}) = \Sigma_\alpha^2 C_\alpha \times [\xi_2(\alpha)] \times {}^2n_\alpha = \Sigma_\alpha^2 A_\alpha \times {}^2 n_\alpha$$

$${}^{111}A(\{\alpha\}) = \Sigma_{\alpha,\beta,\gamma}\Sigma_{\Omega(3)}^{111} C_{\alpha\beta\gamma,\Omega(3)} \times [\xi_1(\alpha) \times \xi_1(\beta) \times \xi_1(\gamma)] \times {}^{111}n_{\alpha\beta\gamma,\Omega(3)} = \Sigma_{\alpha,\beta,\gamma}\Sigma_{\Omega(3)}^{111} A_{\alpha\beta\gamma,\Omega(3)} \times {}^{111}n_{\alpha\beta\gamma,\Omega(3)} \quad (4)$$

where n_α is the number of sites hosting the chemical species defined by the α value; ${}^{11}n_{\alpha\beta,\Omega(2)}$, for instance, is the number of $\alpha\beta$ pairs placed in two sites $r[\Omega(2)]$ apart, and it is the analogue of a two-site interaction; ${}^{111}n_{\alpha\beta\gamma,\Omega(3)}$ refers to the $\alpha\beta\gamma$ triples fixed as a function of their pair distances, and it can be associated to three-site interactions. If one assumes that $A(\{\alpha\})$ is sufficiently approximated by the first three terms of Eq. (4), then

$$A(\{\alpha\}) \approx {}^{0}A + \Sigma_{\alpha}^{1} A_\alpha \times {}^{1}n_\alpha + \Sigma_{\alpha,\beta}\left[{}^{11}A_{\alpha\beta,1} \times {}^{11}n_{\alpha\beta,1} + {}^{11}A_{\alpha\beta,2} \times {}^{11}n_{\alpha\beta,2} + \cdots + {}^{11}A_{\alpha\beta,W} \times {}^{11}n_{\alpha\beta,W}\right] \quad (5a)$$

where ${}^{11}n_{\alpha\beta,1}$, ${}^{11}n_{\alpha\beta,2}$……, ${}^{11}n_{\alpha\beta,\mathrm{W}}$ are the numbers of two-site clusters defined by the pair distances $r[\Omega_1(2)] < r[\Omega_2(2)] < \cdots < r[\Omega_2(W)]$, i.e. first–second…, Wth-order shells. The coefficients ${}^{0}A, {}^{1}A_\alpha, {}^{11}A_{\alpha\beta,1}, {}^{11}A_{\alpha\beta,2} \ldots {}^{11}A_{\alpha\beta,\mathrm{W}}$ depend in general on composition, and can be Taylor expanded in terms of

$${}^{lq}A_{\alpha\beta,W} = {}^{lq}A_{0,\alpha\beta,W} + \Sigma_{\gamma}^{lq} A_{0,\gamma,\alpha\beta,W} \times x_\gamma + \cdots \quad (5b)$$

where x_γ's are composition variables, such as the usual mole fractions of each component.

Mixing energy

The composition of a solid solution formed by two end-members, a and b, is described in terms of their mole fractions, i.e. x_a and x_b. A given composition is in turn compatible with many configurations (Λ), i.e. structure arrangements of the atoms involved in the mixing. The partition function of a solid solution allows one to infer the thermodynamic properties of the related system and can be written as

$$Z(T, x_a, x_b) = \Sigma_\Lambda \exp[-E(x_a, x_b, \Lambda)_{LT}/kT] \times Z(T, x_a, x_b, \Lambda)_{vib}, \quad (6)$$

where k = Boltzmann constant, LT = lattice energy and vib = atomic vibrations dependent component of the partition function. Note that we are assuming that room pressure renders it reasonable to neglect $P \times V(x_a,x_b,\Lambda)$ and use therefore the NVT ensemble. In our case, we have observed that $Z(T,x_a,x_b,\Lambda)_{vib}$, in the limit of the harmonic approximation (1) yields a small contribution to the Helmholtz free energy, F, in comparison with its lattice counterpart (see "Parametrization of the mixing/excess Helmholtz free energy" section) and (2) is comparatively little sensitive to configuration (sampling over different configurations shows $\sigma(F_{\mathrm{vib}})/\langle F_{\mathrm{vib}}\rangle \ll 1$ %). In this view, we have chosen to replace $Z(T,x_a,x_b,\Lambda)_{vib}$ with its zero-order approximation, i.e. $\langle Z(T,x_a,x_b,\Lambda)_{\mathrm{vib}}\rangle_{\Lambda\text{-configurations}} = Z(T,x_a,x_b)_{vib}$, which depends on composition only. Equation (6) is therefore decoupled and factorized in terms of

$$Z(T, x_a, x_b) \approx \Sigma_\Lambda \exp[-E(x_a, x_b, \Lambda)_{LT}/kT] \times Z(T, x_a, x_b)_{vib} = Z(T, x_a, x_b)_{LT} \times Z(T, x_a, x_b)_{vib},$$

and the Helmholtz free energy turns out to be

$$F(T, x_a, x_b) = -k \times T \times \ln\left[Z(T, x_a, x_b)_{LT}\right] - k \times T \times \ln\left[Z(T, x_a, x_b)_{vib}\right].$$

F can be split into the following contributions:

$$F = F_{LT} + F_{HT} + F_{Hpz} + F_A,$$
$$F_{LT} = -k \times T \times \ln\left[Z(T, x_a, x_b)_{LT}\right],$$
$$F_{HT} + F_{Hpz} + F_A = -k \times T \times \ln\left[Z(T, x_a, x_b)_{vib}\right],$$

where the subscripts stand for HT = explicitly T-dependent harmonic energy, Hpz = zero point energy, A = anharmonic contribution; HT and Hpz contributions are determined by atomic vibration frequencies from lattice dynamics formalism.

For a solid solution of two end-members, one writes

$$F(T, x_a, x_b) = x_a \times F(T)_a + x_b \times F(T)_b + \Delta F(T, x_a, x_b)_{\mathrm{mixing}}, \quad (7)$$

where $F(T)_j$ is the contribution of the jth end-member to F and the linear part of the right-hand side of the equation above accounts for a Vegard-like term, whereas $\Delta F(T,x_a,x_b)_{\mathrm{mixing}}$ represents the "mixing" free energy and cancels out at the ends of the join. Such term of Eq. (7) can be further split as follows:

$$\Delta F(T, x_a, x_b)_{\mathrm{mixing}} = \Delta F(x_a, x_b)_{\text{LT-mixing}} + \Delta F(T, x_a, x_b)_{\text{HT-mixing}} + \Delta F(x_a, x_b)_{\text{Hpz-mixing}} + \Delta F(T, x_a, x_b)_A.$$

The partition function related to the lattice configuration part of the mixing free energy of a solid solution is

$$Z(T, x_a, x_b)_{\text{LT-mixing}} = \Sigma_\Lambda \exp[-\Delta E(x_a, x_b, \Lambda)_{\text{LT-mixing}}/kT], \quad (8a)$$

where

$$\Delta E(x_a, x_b, \Lambda)_{\text{LT-mixing}} = E(x_a, x_b, \Lambda)_{LT} - x_a \times E_{LT,a} - x_b \times E_{LT,b},$$

$E_{LT,a-b}$ being the end-members' static lattice energies, and therefore,

$$\Delta F(T, x_a, x_b)_{\text{LT-mixing}} = -k \times T \times \ln[Z(T, x_a, x_b)_{\text{LT-mixing}}]. \quad (8b)$$

Moreover,

$$Z(T,x_a,x_b)_{\text{LT-mixing}} = N_{\text{config}} \times \left\{\left(1/N_{\text{config}}\right) \times \Sigma_\Lambda \exp[-\Delta E(x_a,x_b,\Lambda)_{\text{LT-mixing}}/kT]\right\} = N_{\text{config}} \times z(T,x_a,x_b)_{\text{LT-mixing}}, \quad (8c)$$

where $N_{\text{config}} = N_{\text{Avogadro}}!/[(x_a \times N_{\text{Avogadro}})!\,(x_b \times N_{\text{Avogadro}})!]$.

All calculations related to the lattice energy have been carried out by quantum mechanical methods, using the CRYSTAL code (Dovesi et al. 2009). Among the earlier works in which such code is used to treat thermodynamics of solid solutions, though with different approach, we mention here Meyer et al. (2009) and Scanavino and Prencipe (2013).

$\Delta F(T,x_a,x_b)_{\text{HTpz-mixing}} = F(T,x_a,x_b)_{\text{HT}} + E(x_a,x_b)_{\text{Hpz}} - x_a \times F(T)_{\text{HT},a} - x_b \times F(T)_{\text{HT},b} - x_a \times F_{\text{Hpz},a} - x_b \times F_{\text{Hpz},b}$, in turn, has been calculated by means of standard statistical mechanics via atomic vibration frequencies determined by harmonic lattice dynamics, using the GULP program (Gale 1997), adopting the configuration sampling scheme that is being discussed in the computational section and neglecting the anharmonic part. $\Delta F(T,x_a,x_b)_{\text{HTpz-mixing}}$ is obtained as $\langle \Delta F(T,x_a,x_b,\Lambda)_{\text{HTpz-mixing}} \rangle_{\Lambda\text{-configurations}}$ that corresponds to a zero-order approximation. For the sake of simplicity, we describe hereafter the solid solution's composition by x_{Fe} only, which indicates the molar fraction of FeO, and hence,

$$\Delta F(T,x_{Fe})_{\text{mixing}} = \Delta F(T,x_{Fe})_{\text{LT-mixing}} + \Delta F(T,x_{Fe})_{\text{HTpz-mixing}}.$$

Lastly, we use the Helmholtz free energy to discuss stability as an approximation of the Gibbs energy, i.e. $\Delta F(T,x_{\text{Fe}})_{\text{mixing}} \approx \Delta G(T,x_{\text{Fe}})_{\text{mixing}}$, neglecting the $P \times \Delta V_{\text{mixing}}$ term that is immaterial to our purposes at room pressure.

Accuracy of the Helmholtz free energy calculation

The calculations here done at high temperature are based on the (Mg,Fe)O structure equilibrated by static relaxation and excluding the F_A contribution. Therefore, one commits two errors due to (1) using a volume value out of equilibrium and (2) making a truncation on energy. Let V and $V + \delta V$ be the equilibrium volume at T and P_r, i.e. room pressure, and the value used for calculations, respectively; then,

$$F(V+\delta V,T)_{LT} + F(V+\delta V,T)_{HT} + F(V+\delta V,T)_{Hpz} + F(V+\delta V,T)_A \approx F(V,T) - \left(\frac{\partial F}{\partial V}\right)_{V,T} \times \delta V = F(V,T) - P_r \times \delta V$$

Manipulating the expression above, one can estimate the total error, δF, committed on free energy as follows:

$$\delta F = F(V,T) - F(V+\delta V,T)_{LT} - F(V+\delta V,T)_{HT} - F(V+\delta V,T)_{Hpz} \approx P_r \times \delta V + F(V+\delta V,T)_A. \quad (9)$$

Using the thermal expansion data from Fei (1995), one obtains a figure as large as ~7×10^{-5} kJ/mol, for the former term of the right-hand side of Eq. (9), and ~5×10^{-1} kJ/mol, for the latter one that is estimated as an average over the interval 300–2,500 K (the largest and smallest F_A values are 1.3 and 0.02 kJ/mol; Oganov and Dorogokupets 2003). Above the Neel temperature (T_N), i.e. ~200 K (Kittel 2005), FeO passes from anti-ferromagnetic to paramagnetic; T_N is lower for (Mg,Fe)O because of fewer super-exchange Fe–O–Fe interactions (Speziale et al. 2005). We here model the paramagnetic state as a disordered anti-ferromagnetic spin arrangement. We have determined that the energy differences between (1) ideally anti-ferromagnetic FeO, i.e. having Fe atoms with upward and downward spin orientations in alternate (111) planes; (2) disordered anti-ferromagnetic FeO, i.e. such as the total sum of spins is zero; and (3) ferromagnetic configuration, lie within 1 kJ/mol from each other, and such figure reduces further in Mg–Fe solid solution where the content of iron is smaller than in the FeO end-member. Altogether, on the basis of the discussion above, we take ~1 kJ/mol as an upper estimation of the average uncertainty committed on the ΔF_{mixing} that is being discussed in the ensuing sections. Lastly, note that mixing entropy is not affected by a spin-disorder contribution as that of (Mg,Fe)O, i.e. $x_{\text{Fe}} \times R \times ln\,(2)$, cancels out with FeO's of the Vegard-like part.

Computational

A*b initio* linear-combination-of-atomic-orbitals calculations (HF/DFT-CRYSTAL09 program; Dovesi et al. 2009) have been performed to determine the lattice energy for configurations over the compositional range from periclase to wüstite, relaxing the structure to its equilibrium at ambient pressure and 0 K. A Hamiltonian based on the WC1LYP scheme (Scanavino et al. 2012), which contains a hybrid Hartree–Fock/density functional exchange–correlation term that mixes the WCGGA exchange component (Wu and Cohen 2006) with the exact nonlocal HF exchange contribution and models correlation energy via the Lee–Yang–Parr GGA functional (Lee et al. 1988), has been adopted in the present work.

Several schemes of hybridization rate ($\Im$: Hartree–Fock fraction of exchange energy) have been tested, in the wake of Alfredsson et al. (2004) who have discussed how $\Im$ affects the ability to model specific properties. We have here tried out hybridization models using $\Im$ constant and $\Im$ dependent on composition, $\Im_x$. In the end, we have chosen to adopt the unorthodox approach based on $\Im_x$. Note that Cremer (2001) provides a thorough survey over the role of hybridization and the contributions it yields to exchange energy of a multi-electron system as a function of the functional used, paying special attention to the BLYP-class.

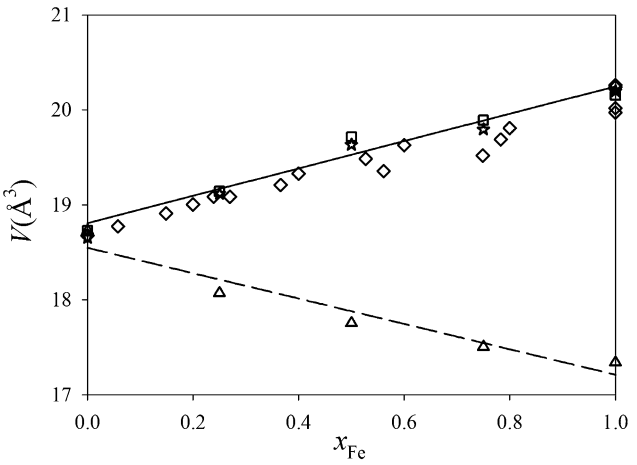

Fig. 1 Primitive cell volume (Å^3) as a function of composition. *Empty diamonds* refer to experimental data on quasi-stoichiometric (Zhang 2000; Fjellvag et al. 1996) and non-stoichiometric (Jacobsen et al. 2002; Simons 1980; Rosenhauer et al. 1976) (Mg,Fe)O samples. *Empty squares* (linear regression: *full line*) and *triangles* (*dashed line*) represent theoretical volume values for HS and LS configurations, respectively. *Stars* refer to values from HS configuration with hybridization equal to 0.20, by way of example

$\Im_1$ and $\Im_0$ have been chosen as a compromise to correctly reproduce the experimental Γ–Γ electronic energy band gaps, geometry and heat capacity of the end-members (see "Experimental data versus calculations" section; Anisimov et al. 1990; Taurian et al. 1985; $\Im_{MgO} = 0.20$ and $\Im_{FeO} = 0.16$). $\Im_x$, in turn, is supposed to take intermediate values and is expressed as $\Im_x = (1-x_{Fe}) \times \Im_0 + x_{Fe} \times \Im_1 + x_{Fe} \times (1-x_{Fe}) \times \Theta(\Im_0,\Im_1)$. The first two terms of the right-hand side member stand for a Vegard-like contribution to $\Im_x$; the third one accounts for a coupling. $\Theta(\Im_0,\Im_1)$ is taken to be symmetric in $\Im_0$ and $\Im_1$, and such that it cancels for both $\Im_0 = 0$ and $\Im_1 = 0$. This has led us to consider expansions based on $A_\alpha \times (\Im_0 \times \Im_1)^\alpha$ terms, where α's are generic exponents and A_α the related coefficients. Following a trial-and-error scheme, aimed at giving Mg–Fe solid solutions' electronic energy gap values well fitted ($R = 0.997$) by Eq. (8) of Zhao et al. (2012), see also Hill (1974), and smooth curves of mixing properties as a function of x_{Fe}, we have concluded that $\alpha = 1$, and $A_\alpha = 1$ is a satisfactory choice for the purposes of this work. Our choice of following an $\Im_x$-based approach is dictated by a wealth of preliminary tests we did using 27 and 8-cation super-cells, in which constant hybridization rates have been explored, from 0.15 to 0.20. In so doing, we observed that (all the quantities mentioned below are obtained as averages over 6–12 independent configurations.): (1) the cell volumes delivered by the different $\Im$ formulations do not change significantly from each other and with respect to the available experimental values (Fig. 1); (2) the Γ–Γ E_{gap} trends show features that range from incongruous to congruous with respect to those expected in alloys or semiconducting systems based on solid solutions, and $\Im_x$ gives the best results. By way of example, fitting the Zhao et al. (2012) function to our E_{gap}'s obtained by $\Im = 0.16$ (yielding the best results among calculations with constant hybridization rate) and $\Im_x$, one has $R = 0.940$ and 0.997, and t(Student) = 12 and 36, respectively. However, the ΔE (corresponding to solid solution's lattice energy from which the Vegard part is subtracted) trend as a function of x_{Fe} with constant hybridization rate exhibits characters in contrast with observations (Baiocchi et al. 2001), and points to a remarkable difficulty to replace Mg with Fe and modest easiness for the reverse exchange; (3) inferences about the *T*–*X* phase relations diagram show consistency with experimental evidences or expectations from other investigations (for instance: temperature of solid solution's stability, critical temperature, and spinodal/binodal decompositions. See "Results and discussion" for references about) only if one takes $\Im_x$. We are conscious of the heuristic character of the way chosen to treat hybridization, which, although it has proven the only one able to yield consistent results for (Mg,Fe)O, yet requires a solid statistical basis over more materials for a substantiation and generalization.

The following values have been used for the tolerances governing the accuracy of the integrals of the self-consistent-field cycles: 10^{-6} for coulomb overlap, 10^{-6} for coulomb penetration, 10^{-6} for exchange overlap, 10^{-6} for exchange pseudo-overlap in direct space and 10^{-12} for exchange pseudo-overlap in reciprocal space. A threshold of 10^{-9} a.u. has been chosen for SCF cycles' convergence, replaced by a 10^{-10} threshold for frequencies calculation. The reciprocal space has been sampled according to a regular sub-lattice with a shrinking factor IS equal to 12 and corresponding to 189 k points throughout the irreducible Brillouin zone. The structure relaxation has been assumed to converge when ∇E, i.e. gradient of energy at atomic positions, and $\boldsymbol{D}_s$, i.e. the related atomic displacements vector, have root mean square and largest component smaller than chosen thresholds, i.e. 0.00120–0.00180 and 0.00030–0.00045 a.u., respectively.

The Mg basis set has been taken from Causà et al. (1986) and extended by the addition of diffuse *sp* and *d* shells so as to obtain a 85-11G* contraction; the original O basis set is that of Ottonello et al. (2008, 2010) modified by the addition of a *d* shell to obtain a 84-11G* contraction; the basis set of Valerio et al. (1995) has been adopted for Fe corresponding to a 86-41G* contraction scheme. A re-optimization of the exponents of the outer Gaussian functions of Fe–Mg–O has been performed.

Solid solutions have been modelled by 64-cation sites super-cells, in which random Mg–Fe occupations have been simulated for a total of 40–50 independent magnesium–iron arrangements with compositions strewn between

Table 1 Interaction parameters (Hartree), as in Eq. (10)

HS			
	$^{0}A_{0}$	$^{0}A_{0,Fe}$	
	1.2638646E − 02	−1.915913E − 03	
I-shell	II-shell	III-shell	IV-shell
$^{11}A_{0,Fe-Mg,1}$	$^{11}A_{0,Fe-Mg,2}$	$^{11}A_{0,Fe-Mg,3}$	$^{11}A_{0,Fe-Mg,4}$
−3.031710E − 04	−1.980510E − 04	−1.484700E − 05	−5.777800E − 05

$^{0}A_{0}$, $^{0}A_{0,Fe}$ (Hartree/atom) and $^{11}A_{0,Fe-Mg,n}$ (Hartree/pair) parameters as in Eq. (10). Hartree to kJ/mol conversion factor = 2,625.5. They refer to the HS model only, as it is the one making physical sense at room pressure

$x_{Fe} = 0$ and 1. Pure HS or LS iron states have been simulated, leaving aside mixed configurations. In the case of the HS configuration, the paramagnetic state has been modelled by disordered anti-ferromagnetic Fe arrays (see "Accuracy of the Helmholtz free energy calculation" section). Expansions like Eq. (5a, b) have been fitted to the lattice energy difference between each Mg/Fe configuration and the related Vegard contribution to determine the $^{l}A_{0,\alpha}$ and $^{lm}A_{0,\alpha\beta}$ parameters. Taking into account that x_{Fe} is the only independent composition variable, given that $x_{Mg} = 1-x_{Fe}$, we have eventually gathered of adopting the expression beneath

$$x_{Fe} \times (1 - x_{Fe}) \times [^{0}A_{0} + {}^{0}A_{0,Fe} \times x_{Fe}] + [{}^{1}A_{0} + {}^{1}A_{0,Fe} \times x_{Fe}] + \Sigma_{j=1,4}^{11} A_{0,Fe-Mg,j} \times {}^{11}n_{Fe-Mg,j} \quad (10)$$

Equation (10) is composed of (1) a first term such as to fulfil $lim_{x\to 0,1}{}^{0}A(x_{Fe}) = 0$ (see also Ferreira et al. 1988); (2) a linear residue, $^{1}A(x_{Fe})$, which acts as a Vegard-like correction to account for deviations from quadratic/cubic/etc. x_{Fe} forms and is then excluded for pure mixing energy calculations; and (3) a series of pair interaction terms. Note that Eq. (10) was chosen after tests made using shells from 2 to 12 Å, and seeking for as simple an expression as possible. In so doing, we have observed that Eq. (10) (i.e. truncation up to 5.5 Å) provides for (Mg,Fe)O's mixing lattice energy a description numerically comparable to that achievable by more shells and a more complex x_{Fe} dependence of the A_0 coefficients, which turn out to be highly correlated with each other. Table 1 displays the HS state's A_0 coefficients (for the sake of brevity we show HS, only, it being the spin configuration that makes sense at low pressures), which lead to a quasi-regular MgO–FeO solid solution; note that such conclusion would be achieved, for the present instance, even using an extended expansion with composition dependent coefficients.

We have then simulated, for a given composition, random Mg/Fe configurations in 1728-cation sites super-cells and, via the A_0s of Table 1, calculated the related $\Delta E(x_a,x_b,\Lambda)_{LT\text{-}mxing}$ values, which have then allowed one to build the Helmholtz free energy. The super-cell's size has been chosen on the basis of tests with $x_{Fe} = 0.5$ in order that an increase of the mixing sites' number does not significantly affect the Helmholtz free energy. $z(T,x_a,x_b)_{LT\text{-}mixing}$ of Eq. (8c) has been estimated by generating different random configurations, whose summation has been truncated according to the ensuing principle. Let us indicate by $\Delta F(T_0,x_{Fe})_{LT\text{-}mixing(N)}$ the free energy attained using N random configurations; when the ratio between expected standard deviation and average value over the set given by $\{\Delta F(T_0,x_{Fe})_{LT\text{-}mixing(M)}$; with $T_0 = 300$ and 2,000 K; $N < M < N + 1{,}000$ and $N > 10^{6}$–$10^{8}\}$ is smaller than 10^{-7}, convergence is assumed to be achieved.

Calculations of thermal properties involving atomic vibrations have been carried out by GULP (Gale 1997), using for Fe–Fe, Fe–O, Mg–Mg, Mg–O and O–O the Buckingham-type interaction potentials from the program's repository (Lewis and Catlow 1985). Such an approach is not able to distinguish between spin states and provides an average description only. For each composition explored, we have performed calculations to model the atomic vibrations dependent part of the Helmholtz energy adopting a 4 × 4 × 4 sampling grid in the reciprocal space and 216-cation sites super-cells. The generation of different configurations has been interrupted following a criterion similar to the one discussed above, though with a less dense sampling (~15,000–20,000 configuration points, as a function of composition). Further calculations of thermal properties have been carried out for the sake of completeness using also the ab initio approach, but paying attention to the end-members only, on account of the huge computing time required to achieve a statistical representativeness and the comparatively small contribution of the vibrational terms with respect to lattice energy.

Results and discussion

Experimental data versus calculations

In Fig. 1, the primitive cell volume, V, is displayed as a function of x_{Fe}. Measured V values (Jacobsen et al. 2002; Zhang

2000; Fjellvag et al. 1996; Simons 1980; Rosenhauer et al. 1976) refer to quasi-stoichiometric and non-stoichiometric samples; whereas, the theoretical volumes, determined by static energy structure relaxation, are shown for HS and LS configurations. LS leads to a shrinking of V upon an enrichment in Fe, at variance with observations at room pressure; HS yields results in good agreement with experiments, in particular for Mg-rich compositions. An overestimation of volume with respect to measurements seems to affect the V predictions for Fe-rich structures; we are inclined to think this might be reflective of the samples' non-stoichiometric character, which leads to smaller Vs than the ideally stoichiometric counterparts'. The pressure contribution due to vibrational energy and zero point energy yields negligible V value corrections, estimated of about 0.001–0.002 Å^3.

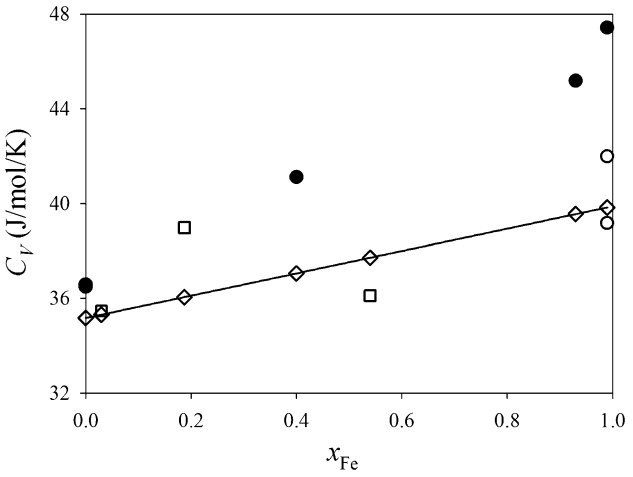

Fig. 2 Heat capacity values at constant volume (J/mol/K) and room temperature, over the MgO–FeO join. *Empty diamonds* (linear regression: *full line*): data from semi-empirical simulations; *empty circles* issues of quantum mechanical modelling. Experimental determinations are shown by *filled circles*, whereas *empty squares* stand for theoretical values other than ours

Figure 2 shows a comparison between the room temperature heat capacity values at constant volume (C_V) here determined by the CRYSTAL (for end-members only) and GULP codes via lattice dynamics and statistical mechanics, and those predicted by other authors (Scanavino et al. 2012; Wu and Cohen 2006) or measured (Zhang and Kostak 2002; Grønvold et al. 1993; Stølen et al. 1996). We confine the present analysis to the HS configuration that we have proven above to provide physical $V(x_{Fe})$ trends at room pressure. C_V values exhibit a considerable scattering, in our opinion because of the likely non-stoichiometric character of Fe-bearing samples and consequent defectiveness. Observed C_V of quasi-wüstite differs from the predicted ones by 9, 15 and 14 %, for HS, LS and semi-empirical modelling, respectively. In the case of MgO, for which reliable and abundant data are available, the degree of accord between our determinations and experimental issues is satisfactory. Figure 3 reports a comparison between the observed and calculated $C_V(T)$ curves. Experimental $C_P(T)$ values (Holland and Powell 1998) have been converted into $C_V(T)$s by the classic thermodynamic relationship linking $C_P(T)$ to $C_V(T)$ via volume thermal expansion (Dubrovinsky and Saxena 1997; Fei 1995) and bulk modulus (Scanavino et al. 2012; Fei 1999). The discrepancy between measurements and calculations, estimated over the interval for which we have been able to find experimental data, amounts to 0.3 %, in the case of semi-classic modelling, and to 1.2 %, for quantum mechanical simulations. As to the entropy calculations, MgO experimental $S^{298\ K}$, i.e. 26.9 J/mol/K (Kubaschewki et al. 1993), is

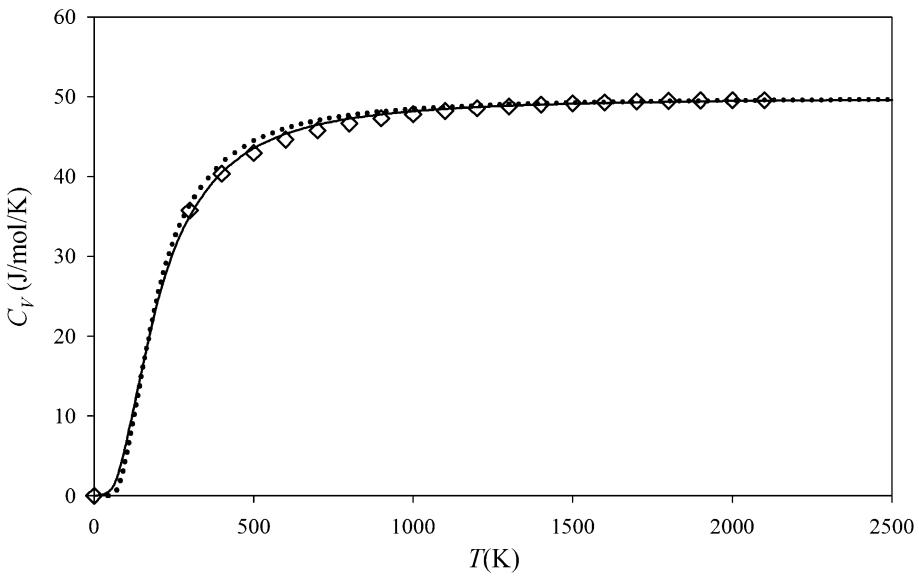

Fig. 3 Heat capacity at constant volume (J/mol/K) of MgO as a function of temperature. Experimental data (*empty diamonds*) have been attained from the Holland and Powell (1998) data base. C_P is converted into C_V using bulk modulus and volume thermal expansion from Fei (1995, 1999 and Dubrovinsky and Saxena (1997). *Full line* C_V from semi-empirical calculations; *dotted line* C_V from LS quantum–mechanical modelling

Table 2 Helmholtz free energy (kJ/mol) as a function of composition and temperature (K)

	p_0	p_1	p_2
$\Delta F_{LT-excess} = x \times y \times \left[U_0(T) + U_1(T) \times (x-y) + U_2(T) \times (x-y)^2\right] Z$			
HS			
$U_0(T)$	18.2043182144	0.0000936572182865	−0.0000000243421184957
$U_1(T)$	0.357364723303	−0.00000691673540265	0.0000000178134134229
$U_2(T)$	−1.33522525326	−0.0000536329464692	0.0000000136172021797
LS			
$U_0(T)$	28.4445905153	0.000253581685406	−0.000000065391665275
$U_1(T)$	−11.257466176	−0.00711243288403	−0.000000321846428917
$U_2(T)$	−25.052895446	−0.0143218654633	−0.000000618753883058
$\Delta F_{excess} = x \times y \times \left[U(T)_0 + U(T)_1 \times (x-y) + U(T)_2 \times (x-y)^2\right] Z$			
HS			
$U_0(T)$	17.3682200605	−0.00125828910357	−0.000000254046117247
$U_1(T)$	0.551495057519	0.000269405967138	0.0000000478722696912
$U_2(T)$	−0.48873957368	0.00119708716955	0.000000204305028065

x is the mole fraction of FeO; $y = 1 - x$. See text for definition of $U_j(T)$

The use of a large number of digits allows an accurate reproduction of the curves here discussed

to be compared with 24.4 J/mol/K, from semi-empirical modelling, and 23.5 J/mol/K, from ab initio.

Parametrization of the mixing/excess Helmholtz free energy

Mixing free energy has been parametrized as a function of x_{Fe} and T, using a composition–temperature grid over the full FeO–MgO join and ranging from 50 to 3,000 K. Such a choice is due to our aim of providing a deliverable useful for any further application requiring thermo-chemical energy values. In so doing, we have chosen to expand the actual field of stability to guarantee a smooth interpolation, free of discontinuities at the boundaries.

Over the interval 50–3,000 K, $\Delta F(T,x_{Fe})_{HTpz\text{-}mixing}$ contributes on average to $\Delta F(T,x_{Fe})_{mixing}$ for $x_{Fe} = 0.25$, 0.50, and 0.75 in terms of 13, 17 and 10 %, respectively, with the largest figure smaller than 2 kJ/mol, which is of the same magnitude of the uncertainty discussed in "Computational" section. This aspect, along with that $\Delta F(T,x_{Fe})_{HTpz\text{-}mixing}$ has been calculated by a semi-empirical approach, suggests to pay due care in using the harmonic contribution to the Helmholtz free energy; in such a light, we have chosen to separately discuss the composition–temperature thermo-chemical properties derived from mixing lattice energy only and those from total mixing energy. Yet note that even a small contribution to mixing free energy may have relevant bearings on the T–X phase relation diagram and critical temperature.

Given that $\Delta F(T,x_{Fe})_{HTpz\text{-}mixing} < 0$ for any composition and temperature explored, we gather the harmonic part of the mixing free energy promotes formation of solid solution, which is, in some cases, stymied, in other cases, boosted by $\Delta F(T,x_{Fe})_{LT\text{-}mixing}$ that takes positive and negative values as a function of T and x_{Fe}.

We tested several $x_{Fe}y_{Mg}$ function to model mixing free energy and observed that the one giving the most satisfactory results, in terms of fitting figures of merit in combination with formal simplicity, is the Redlich–Kister-type expression (Stølen and Grande 2004)

$$\begin{aligned}\Delta F(T,x_{Fe})_{mixing} &= x_{Fe} \times y_{Mg} \times [U_0(T) + U_1(T) \times (x_{Fe} - y_{Mg}) \\ &\quad + U_2(T) \times (x_{Fe} - y_{Mg})^2] \\ &\quad + R \times T \times \left[x_{Fe} \times \ln(x_{Fe}) + y_{Mg} \times \ln\left(y_{Mg}\right)\right],\end{aligned}$$

where

$$y_{Mg} = 1 - x_{Fe},$$

$$\begin{aligned}\Delta F(T,x_{Fe})_{excess} = x_{Fe} \times y_{Mg} \times [U_0(T) + U_1(T) \\ \times (x_{Fe} - y_{Mg}) + U_2(T) \times (x_{Fe} - y_{Mg})^2],\end{aligned}$$

and

$$U_j(T) = \Sigma_{k=0,2} p_{jk} \times T^k.$$

In Table 2, the p_{jk} parameters are set out for $\Delta F(T,x_{Fe})_{LT\text{-}mixing}$, using the HS and LS models, and $\Delta F(T,x_{Fe})_{mixing}$, restricted to the HS configuration given that (1) it is the one making sense at room pressure and (2) one can derive LS-$\Delta F(T,x_{Fe})_{mixing}$

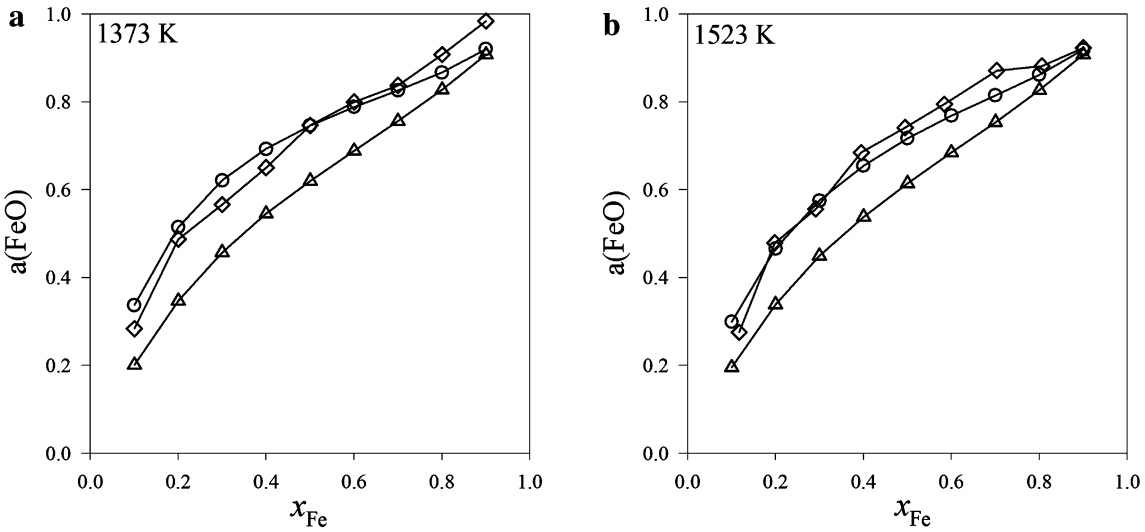

Fig. 4 **a**–**b** Activity–composition relation at **a** 1,373 and **b** 1,523 K, obtained in this study (*empty circles*) compared to experimental results from emf measurements: empty diamonds refer to Hasegawa et al. (2006) and *empty triangles* to Sreçec et al. (1987)

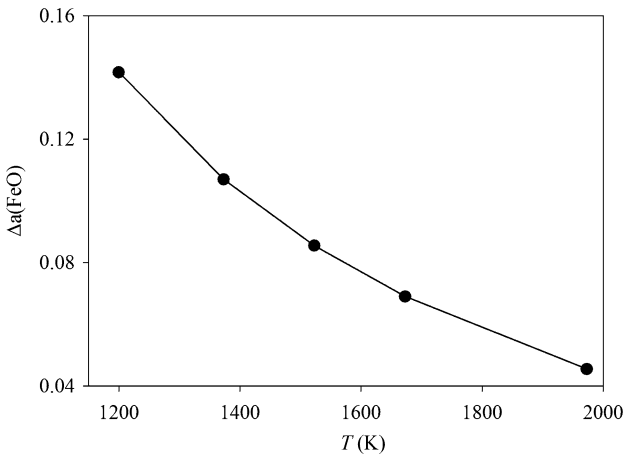

Fig. 5 Temperature dependence of the averaged discrepancy between the activity obtained in the present study and those obtained by Sreçec et al. (1987)

as LS-$\Delta F(T,x_{Fe})_{LT\text{-mixing}}$ + [HS-$\Delta F(T,x_{Fe})_{mixing}$−HS-$\Delta F(T,x_{Fe})_{LT\text{-mixing}}$]. Note that hereafter we address the ideal mixing entropic contribution, i.e. $-R \times [x_{Fe} \times ln(x_{Fe}) + y_{Mg} \times ln(y_{Mg})]$, by $S(x_{Fe})_{ideal\ mixing}$.

First of all, one observes that the HS model yields ΔF values systematically smaller than the ones derived for LS, this pointing to that the former better promotes (Mg,Fe)O solid solution. Note that HS provides absolute energy smaller than LS, and therefore, HS leads to a definitely more stable magnesio-wüstite system, at room pressure.

$\Delta F(T,x_{Fe})_{excess}$ has allowed one to determine the activity of the FeO, which has then been compared with values obtained from emf (electromotive force) and gas measurements by Sreçec et al. (1987) and Hasegawa et al. (2006). Figure 4a, b display at 1,373 and 1,573 K our results from computational modelling and experimental data. Theoretical modelling provides activity figures that lie in-between the experimental curves, in slightly better agreement with Hasegawa's issues (average discrepancy 4 %) than Sreçec's (average discrepancy 14 %). Using data from Sreçec only, Fig. 5 shows that the disagreement between theoretical and observed activity decreases upon increasing T. We think this is attributable to that the semi-empirical potentials used to model the vibrational contribution have not been optimized and partly fail to reproduce with precision low-frequency modes, important at modest temperatures and sensitive to the quality of the force field. Things improve at high temperature where error compensations can occur owing to involvement of an ever wider vibrational range.

Figure 6 shows the Helmholtz energy curves as a function of T and composition, for static-ΔFs, calculated by LS and HS, and total mixing free energy with HS state, respectively. LS-$\Delta F(T,x_{Fe})_{LT\text{-mixing}}$ undergoes a positive-to-negative energy change between 1,000 and 1,300 K, while the HS model predicts such a crossover on the interval 600–900 K. This latter issue is in keeping with the attainments of Yao et al. (2013), who observe formation of magnesio-wüstite solid solution at some 773 K. HS-$\Delta F(T,x_{Fe})_{mixing}$, in turn, points to a stabilization of the Mg–Fe solid solution over the range 600–800 K, consistently with HS-$\Delta F(T,x_{Fe})_{LT\text{-mixing}}$. Such aspect is reflective of the stabilizing action on (Mg,Fe)O of the vibration-dependent ΔF-component, as stated above. Taking then into account that $\Delta F(T,x_{Fe})_{HTpz\text{-mixing}} < 0$, $-T \times S(x_{Fe})_{ideal\ mixing} < 0$ and

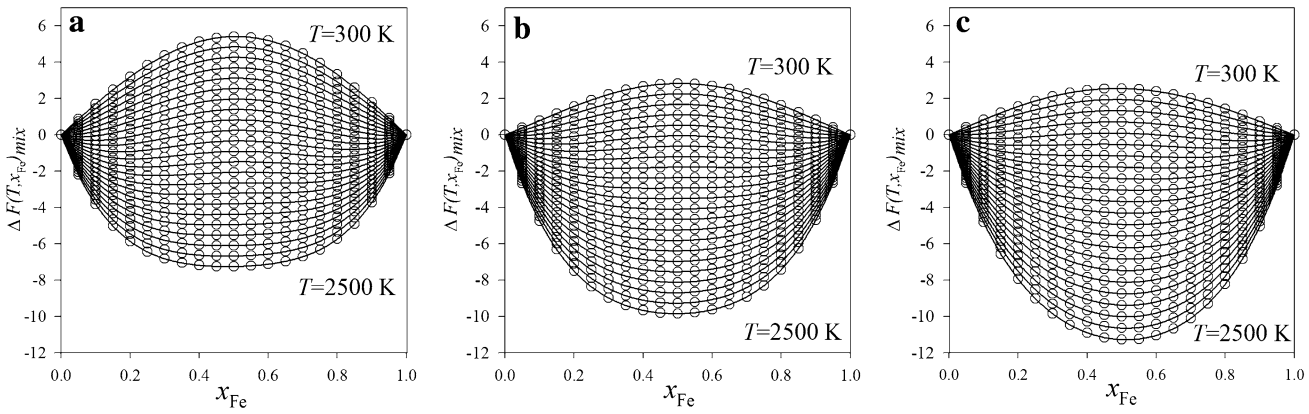

Fig. 6 **a–c** $\Delta F(T,x_{Fe})_{LT\text{-}mixing}$ from the LS (**a**) and (**b**) HS models. $\Delta F(T,x_{Fe})_{mixing}$ determined using the HS state (**c**). Isotherms are spaced by 100 K

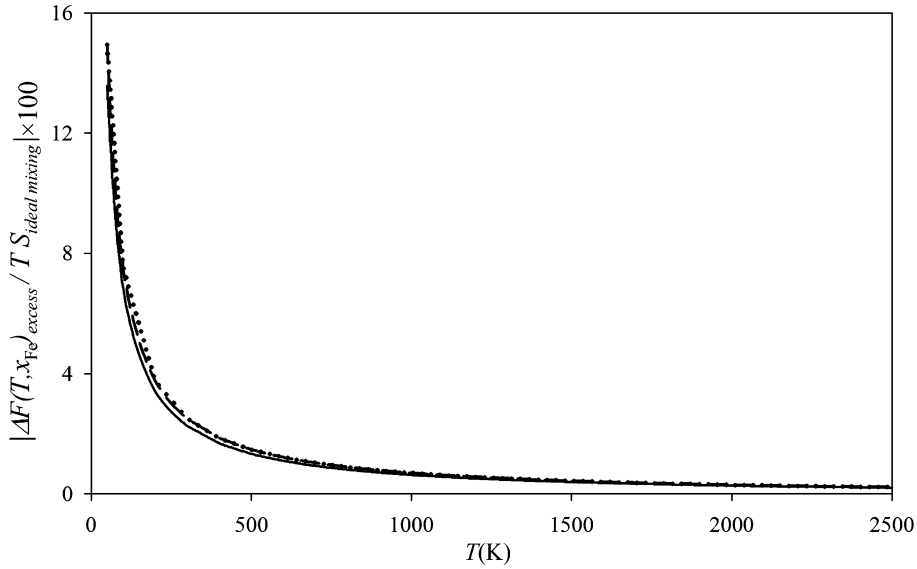

Fig. 7 $|\Delta F(T,x_{Fe})_{excess} / T \times S_{ideal}\ \text{mixing}| \times 100$ as a function of temperature. *Full line*, *dashed line* and *dotted line* refer to $x = 0.25$, 0.50 and 0.75, respectively. Calculations performed by the HS model

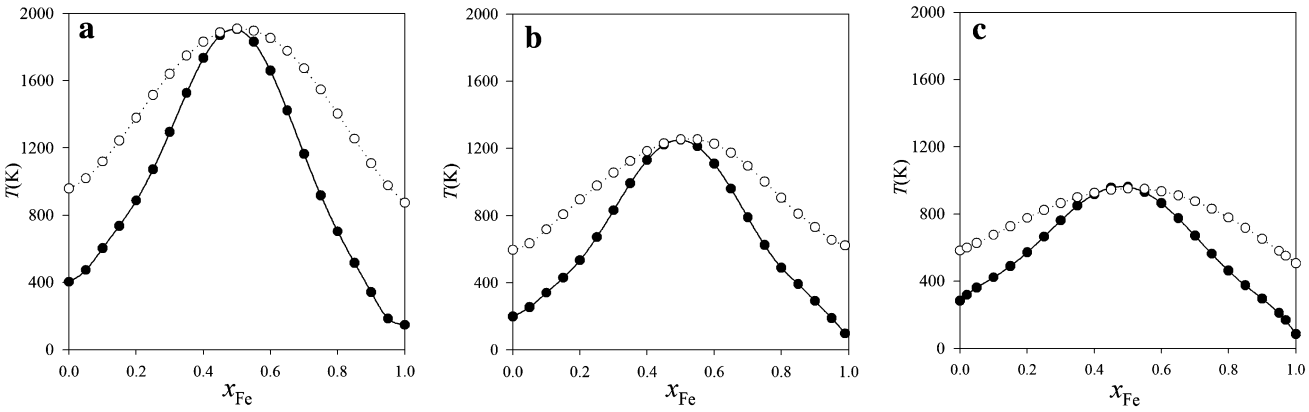

Fig. 8 **a–c** Temperature–composition phase diagram of the system MgO–FeO, predicted using LS-$\Delta F(T,x_{Fe})_{LT\text{-}mixing}$ (**a**), HS-$\Delta F(T,x_{Fe})_{LT\text{-}mixing}$ (**b**) and HS-$\Delta F(T,x_{Fe})_{mixing}$ (**c**). *Empty* and *filled circles* represent binodal and spinodal decomposition temperatures. Composition region of confidence: $0.2 < x_{Fe} < 0.8$

$\Delta F(T,x_{Fe})_{mixing}$ is positive/negative as a function of temperature, it ensures that the pure static energy contribution tends to favour de-mixing but it is offset by vibrational and configuration components of $\Delta F(T,x_{Fe})_{mixing}$.

Eventually, the configuration entropy contribution to HS-$\Delta F(T,x_{Fe})_{mixing}$, i.e. $-T \times S(x_{Fe})_{ideal\ mixing}$, plays above 600–650 K a fundamental role in promoting formation of solid solution versus de-mixing, as it is displayed by Fig. 7 that reports the ratio $|\text{HS-}\Delta F(T,x_{Fe})_{excess}/T \times S(x_{Fe})_{ideal\ mixing}| \times 100$ as a function of T, for $x_{Fe} = 0.25$, 0.50 and 0.75.

Phase relations of (Mg,Fe)O versus T

Figure 8a, b show the T–X phase relations diagram obtained by LS and HS configurations, using $\Delta F(T,x_{Fe})_{LT\text{-}mixing}$; binodal and spinodal boundaries attained by the tangent method and sign inversion of the second derivative of mixing free energy versus composition. We estimate a x_{Fe} region of confidence ranging from 0.2 to 0.8. The former predicts full solid solution above 1,800 K, whereas the latter points to a critical temperature (T_c) of some 1,200 K. This reflects the relevant difference in terms of lattice energy of stabilization played by the two spin configurations explored. Figure 8c displays the T–X phase relations diagram generated by HS-$\Delta F(T,x_{Fe})_{mixing}$, which yields a T_c of some 950 K. For the sake of completeness, had one used LS-$\Delta F(T,x_{Fe})_{mixing}$, one would attain a T_c about 1,500 K. More differences between the three phase relations diagrams can be revealed by analysing the position of the binodal boundary with respect to the spinodal one. In particular, one observes that $T_{binodal} - T_{spinodal}$ for a given composition decreases from LS static, to HS static and finally to HS total, taking average values of 439, 280 and 205 K, respectively. This points to that HS-like models predict a more abrupt process of de-mixing, namely a narrower meta-stability thermal interval, than LS does. We have not been able to find out in literature experimental studies on the T–X relations phase diagram of (Mg,Fe)O, at ambient pressure (Fabrichnaya et al. 2004). Experiments at 80 GPa and 1,000 K (Dubrovinsky et al. 2000) proved that (Mg,Fe)O decomposes into quasi-wüstite and a residual (Mg,Fe)O solid solution. Assuming Fe in low-spin state, as it is at 80 GPa, either LS model, whether including vibrational contribution or not, points to a spinodal de-mixing at 1,000 K giving quasi-symmetrical terms, i.e. somewhat of $(Mg_{0.75}Fe_{0.25})O$ and $(Mg_{0.25}Fe_{0.75})O$. Such a discrepancy, i.e. an excess of Mg in the Fe-rich phase, with respect to observations is ascribable, and we deem, either to pressure that is not taken into account in the T–X phase relations diagrams here discussed, or to a model deficiency in reproducing enough asymmetry on the MgO–FeO join.

The behaviour of the Mg–Fe solid solutions in olivine (forsterite–fayalite) and garnet (pyrope–almandine) is here compared with magnesio-wüstite's; such phases have been chosen as in the former Mg–Fe enter octahedral sites, like in (Mg,Fe)O, whereas in the latter they occupy large dodecahedrally coordinated positions. T_c of olivine (see Dachs and Geiger 2007) ranges from values below 373 K up to some 620 K, altogether pointing to figures smaller than

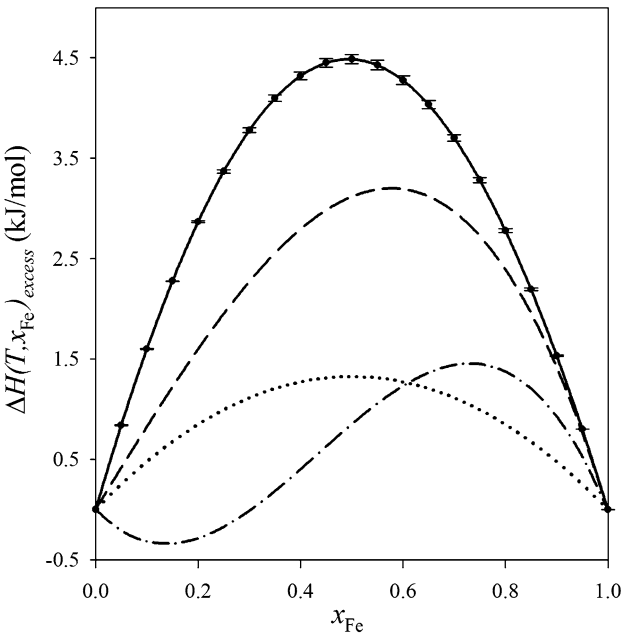

Fig. 9 $\Delta H(T,x_{Fe})_{excess}$, for (Mg,Fe)O: *full line* (present work); $(Mg,Fe)_2SiO_4$: *dashed line* (Wood and Kleppa 1981); $(Mg,Fe)_2SiO_4$: *dotted line* (Kojitani and Akaogi 1994); $(Mg,Fe)_3Al_2(SiO_4)_3$: *dot-dashed line* (Geiger et al. 1987)

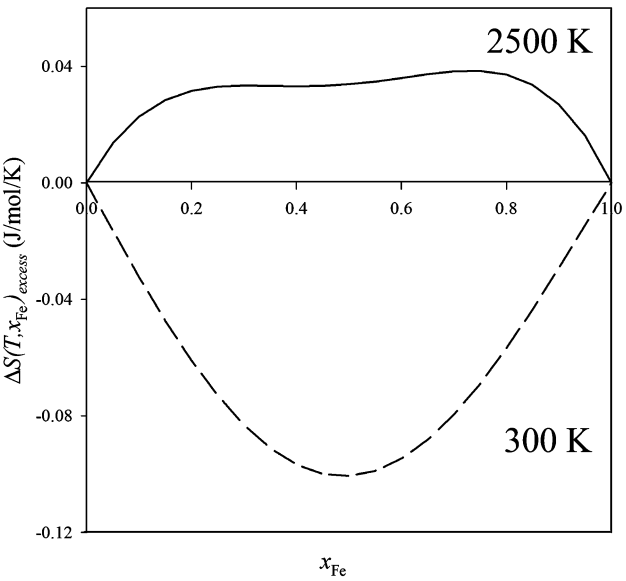

Fig. 10 $\Delta S(T,x_{Fe})_{excess}$ at 300 and 2,500 K, *dashed* and *full line*, respectively

those we have here calculated for (Mg,Fe)O. In the case of Mg–Fe garnets (Ganguly and Kennedy 1974), i.e. pyrope–almandine solid solution, T_c has been estimated of about 750 K, lower than (Mg,Fe)O's as observed for olivine too. We have calculated the excess enthalpy (see Fig. 9) by means of

$$\Delta H(T,x_{\mathrm{Fe}})_{\mathrm{excess}} \approx \Delta E(T,x_{\mathrm{Fe}})_{\mathrm{excess}} = \Delta F(T,x_{\mathrm{Fe}})_{\mathrm{mixing}} - T \times \partial \Delta F(T,x_{\mathrm{Fe}})_{\mathrm{mixing}}/\partial T,$$

using the HS-$\Delta F(T,x_{\mathrm{Fe}})_{\mathrm{mixing}}$ parametrization in Table 2 and neglecting the $P \times \Delta V_{\mathrm{mixing}}$ contribution at room pressure. The bars shown in figure stand for the oscillations of the excess enthalpy values because of temperature and hint that magnesio-wüstite's excess energy is mostly governed by static lattice contributions and its energy levels, for a given composition and as a function of configuration, huddled around an average. In this respect, it is possible the present static approach misses sensitivity in comparison with those methods in which the structure is progressively rearranged, in terms of cation distribution, for equilibration with a temperature, using, for instance, Metropolis-like algorithm, and adding thereby an intrinsic dependence on T not confined to the statistical weight only. $\Delta H(T,x_{\mathrm{Fe}})_{\mathrm{excess}}$ exhibits a quasi-regular trend as a function of composition, corresponding to $W_{\mathrm{H,Mg-Fe}}$, of 17.7(±5) kJ/mol, against a 5.3 kJ/mol for olivine on a one-cation basis (Kojitani and Akaogi 1994), where $\Delta H(T,x_{\mathrm{Fe}})_{\mathrm{excess}} = W \times x_{\mathrm{Fe}} \times (1 - x_{\mathrm{Fe}})$. The quasi-regularity of the MgO–FeO binary is due to that $U_1(T)$, which is the cause of a possible break of symmetry over x_{Fe}, yields a modest contribution in comparison with $U_0(T)$ and $U_2(T)$. Such regular, a behaviour is similar to olivine's, which exhibits a modest sub-regularity characterized by a slight asymmetric bent to Fe-rich compositions according to Wood and Kleppa (1981) and is on the whole regular after Dachs and Geiger (2007). Fe–Mg garnets, in turn, show more marked deviations from regularity, probably even related to the unduly large cage hosting Fe and Mg. For the sake of completeness, we show in Fig. 10 the excess entropy, $\Delta S(T,x_{\mathrm{Fe}})_{\mathrm{excess}}$, determined as $-\partial \Delta F(T,x_{\mathrm{Fe}})_{\mathrm{mixing}}/\partial T - S(x_{\mathrm{Fe}})_{\mathrm{conf}} = -\partial \Delta F(T,x_{\mathrm{Fe}})_{\mathrm{excess}}/\partial T$, using the HS configuration. $\Delta S(T,x_{\mathrm{Fe}})_{\mathrm{excess}}$ ranges from negative to slightly positive values upon increasing T and exhibits absolute figures smaller than 0.1 J/mol/K, to be compared with ideal mixing entropy amounting to 3.9 J/mol/K on average. Note that comparably small values for excess entropy have been found for olivine too (Dachs and Geiger 2007).Thorough discussions about the role of interactions and physical meaning of $\Delta S(T,x_{\mathrm{Fe}})_{\mathrm{excess}}$ are found in Benisek and Dachs (2012), and Stølen and Grande (2004).

Leaving aside any claim of precision, Fig. 11 qualitatively shows how pressure affects the stability of the (Mg,Fe)O solid solution, by analysing the mixing Gibbs energy, $\Delta G(P,T,x_{\mathrm{Fe}})_{\mathrm{mixing}}$, calculated for the HS and LS

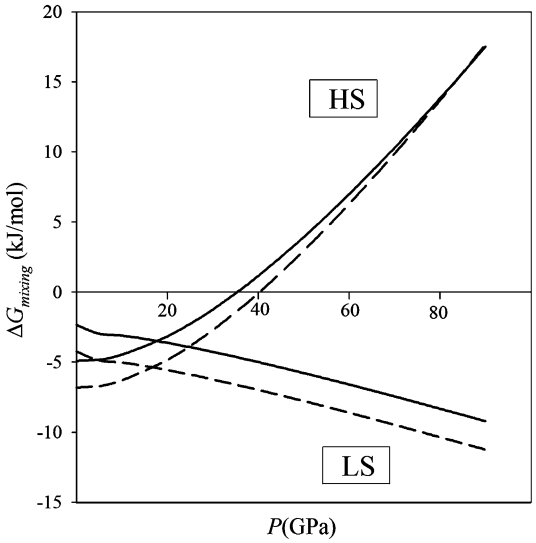

Fig. 11 Mixing Gibbs energy as a function of pressure. *Full line* and *dashed line* correspond to 1,600 and 1,800 K isotherms

models, including the vibrational contributions and with $x_{\mathrm{Fe}} = 0.50$, along the isotherms at 1,800 and 1,600 K (i.e. above T_c whichever model one uses). $\Delta G(P,T,x_{\mathrm{Fe}})_{\mathrm{mixing}}$ can be split in two parts: (1) Δ_{therm}, which has here been modelled and represents the first two terms of the right-hand side of Eq. (1); (2) Δ_{deform}, which accounts for the third term of Eq. (1) and is calculated along an isotherms from room pressure to P, by means of the elastic properties predicted by Persson et al. (2006) and the third order Birch–Murnaghan equation of state. In the low-pressure regime, (Mg,Fe)O solid solution is stable with respect to its end-members, $\Delta G(P,T,x_{\mathrm{Fe}})_{\mathrm{mixing}} < 0$, and the HS configuration is energetically more efficient than LS, because of the Δ_{therm} contribution. At ≈15 GPa and 1,800 K HS-$\Delta G(P,T,x_{\mathrm{Fe}})_{\mathrm{mixing}}$ and LS-$\Delta G(P,T,x_{\mathrm{Fe}})_{\mathrm{mixing}}$ intersect one another, and the LS configuration boosts stability of the (Mg,Fe)O solid solution more effectively than HS. At higher pressure, Δ_{deform} definitely favours the LS configuration and stabilizes (Mg,Fe)O solid solution that grows ever more stable. Conversely, the HS model forecasts a solid solution becoming less and less stable upon growing P with respect to the end-members, as proven by its increasing HS-$\Delta G(P,T,x_{\mathrm{Fe}})_{\mathrm{mixing}}$ trend. At ≈40 GPa, it fails to stabilize magnesio-wüstite, i.e. HS-$\Delta G(P,T,x_{\mathrm{Fe}})_{\mathrm{mixing}} > 0$, which is predicted to decompose into its end-members. The isotherms at 1,600 K trails close to that at 1,800 K and yields similar results; for such a reason, we do not discuss it in detail. In this view, the HS-to-LS transition seems to be a mechanism stabilizing the Mg–Fe solid solution versus de-mixing into end-members at high pressure. Note that more complex de-mixing processes involving decompositions into spinodal (Mg,Fe)O systems, other than end-members,

are here neglected because of the limitation in precision to model pressure induced effects onto the sub-solidus solvi.

Conclusions

The $\Delta F(T,x_{Fe})_{mixing}$ modelled by the HS configuration points to a MgO–FeO solid solution largely controlled by static and configuration contributions, i.e. $\Delta F(T,x_{Fe})_{LT\text{-}mixing}$, in terms of more than 80 %.The modest vibration-dependent component contributes promoting mixing. We have chosen to parameterize $\Delta F(T,x_{Fe})_{mixing}$ as a function of x_{Fe} and T using the following expression:

$\Delta F(T,x_{Fe})_{mixing} = x_{Fe} \times y_{Mg} \times [U_0(T) + U_1(T) \times (x_{Fe} - y_{Mg}) + U_2(T) \times (x_{Fe} - y_{Mg})^2] + R \times T \times [x_{Fe} \times ln(x_{Fe}) + y_{Mg} \times ln(y_{Mg})]$, where $y_{Mg} = 1 - x_{Fe}$ and $U_j(T)$s are polynomials in T of the second order. The $U_1(T)$ function provides a modest contribution to ΔF_{mixing} that has a quasi-symmetric behaviour over the MgO–FeO binary. The sub-solidus solvi exhibits a critical temperature (T_c) of some 950 and 1,200 K, including or neglecting the harmonic part of free Helmholtz energy and using the HS configuration. For the sake of comparison with other minerals hosting Mg–Fe mixing and taking as a reference the former T_c, such a figure is significantly larger than olivine's and Mg–Fe garnet's, wherein Mg–Fe species enter octahedral and dodecahedral sites, respectively. All this points to an Mg–Fe mixing that is more difficult to be stabilized over the MgO–FeO join than that for olivine and garnet. The quasi-regular behaviour of the MgO–FeO binary in high-spin state leads to a ΔH_{excess} that can be modelled by a $x_{Fe} \times (1 - x_{Fe}) \times W$-like function, yielding $W_{H,Mg\text{–}Fe}$ of 17.7(±5) kJ/mol. Excess entropy's absolute figure is smaller than 0.1 J/mol/K and monotonically increases as a function of T. Hence the stability over the sub-solidus join MgO–FeO is mainly governed by lattice energy and ideal mixing entropy. High-pressure and high-temperature conditions favour stabilization of the (Mg,Fe)O solid solution versus end-members with iron in its LS configuration; whereas, the HS model, which is energetically more convenient in the low-pressure regime, ends up promoting decomposition into MgO–FeO surpassing some 40 GPa at 1,800 K. Such conditions correspond to mid lower mantle's and, as a first approximation, are consistent with the observed gradient in the thermal boundary layer 150–300 km above the CMB (Hirose and Lay 2008). All this contributes to the understanding that Mg–Fe mixing and its related spin transition alter the chemical behaviour in the main iron acceptor lower mantle minerals (Mg-wüstite and perovskite), thereby changing the carried iron content via a modification of the partition coefficient between ferropericlase and perovskite (Badro et al. 2003) and impacting onto mantle dynamics through Fe-rich phases' thermo-physical/chemical properties (Lyubutin et al. 2013).

Acknowledgments The present investigation was funded by Italian M.I.U.R through P.R.I.N Grant No. 2010EARRRZ_003. The authors are grateful to Victor Vinograd and to two anonymous referees whose suggestions have really enhanced the quality of the manuscript.

References

Alfredsson M, Price GD, Catlow CRA, Parker SC, Orlando R, Brodholt JP (2004) Electronic structure of the antiferromagnetic B1-structured FeO. Phys Rev B 70:165111–165116

Anisimov VI, Korotin MA, Kurmaev EZ (1990) Band-structure description of Mott insulators (NiO, MnO, FeO, CoO). J Phys Condens Matter 2:3973–3987

Antonangeli D, Siebert J, Aracne CM, Farber DL, Bosak A, Hoesch M, Krisch M, Ryerson FJ, Fiquet G, Badro J (2011) Spin crossover in ferropericlase at high pressure: a seismologically transparent transition? Geophysical Research Abstracts, vol 13, EGU2011-12930

Badro J, Struzhkin V, Shu J, Hemley RJ, Mao HK, Kao CC, Rueff JP, Shen G (1999) Magnetism in FeO at megabar pressures from x-ray emission spectroscopy. Phys Rev Lett 83:1401–1404

Badro J, Fiquet G, Guyot F, Rueff J-P, Struzhkin VV, Vanko G, Monaco G (2003) Iron partitioning in earth's mantle: toward a deep lower-mantle discontinuity. Science 300:789–791

Baiocchi M, Caucia F, Merli M, Prella D, Ungaretti L (2001) Crystal-chemical reasons for the immiscibility of periclase and wüstite under lithospheric P, T conditions. Eur J Miner 13:871–881

Barnard RW, Dahlquist G, Pearce K, Reichel L, Richards KC (1998) Gram polynomials and the Kummer function. J Approx Theory 94:128–143

Bellaiche L, Vanderbilt D (2000) Virtual crystal approximation revisited: application to dielectric and piezoelectric properties of perovskites. Phys Rev B 61:7877–7882

Benisek A, Dachs E (2012) A relationship to estimate the excess entropy of mixing: application in silicate solid solutions and binary alloys. J Alloys Compd 527:127–131

Bennet J, Kwong S (2010) Thermodynamic studies of MgO saturated EAF slag. Ironmak Steelmak 37:529–535

Causà M, Dovesi R, Pisani C, Roetti C (1986) Electronic structure and stability of different crystal phases of magnesium oxide. Phys Rev B 33:1308–1316

Cohen RE, Mazin II, Donald G, Isaak DG (1997) Magnetic collapse in transition metal oxides at high pressure: implications for the earth. Science 275:654–665

Cook SJ, Bowman JR (2000) Mineralogical evidence for fluid–rock interaction accompanying prograde contact metamorphism of siliceous dolomites: alta stock aureole, Utah, USA. J Petrol 41:739–757

Cremer D (2001) Density functional theory: coverage of dynamic and non-dynamic electron correlation effects. Molec Phys 99(23):1899–1940

Crowhurst JC, Brown JM, Goncharov AF, Jacobsen SD (2008) Elasticity of (Mg, Fe)O through the spin transition of iron in the lower mantle. Science 319:451–453

Dachs E, Geiger CA (2007) Entropies of mixing and subsolidus phase relations of forsterite–fayalite (Mg_2SiO_4–Fe_2SiO_4) solid solution. Am Miner 92:699–702

De La Pierre M, Noël Y, Mustapha S, Meyer A, D'Arco P, Dovesi R (2013) The infrared vibrational spectrum of andradite-grossular solid solutions: a quantum mechanical simulation. Am Miner 98:966–976

Dovesi R, Saunders VR, Roetti C, Orlando R, Zicovich-Wilson CM, Pascale F, Civalleri B, Doll K, Harrison NM, Bush IJ, D'Arco P,, Llunell M (2009) CRYSTAL09 User's Manual (University of Torino) Torino

Dubrovinsky LS, Saxena SK (1997) Thermal expansion of periclase and tungsten to melting temperature. Phys Chem Miner 24:547–550

Dubrovinsky LS, Dubrovinskaia NA, Saxena SK, Annersten H, Halenius E, Harryson H, Tutti F, Rekhi S, Le Bihan T (2000) Stability of ferropericlase in the lower mantle. Science 289:430–432

Duffy TS, Hemley RJ, Mao HK (1995) Equation of state and shear strength of magnesium oxide to 227 GPa. Phys Rev Lett 74:1371–1374

Fabrichnaya O, Saxena SK, Richet P, Westrum EF (2004) Thermodynamic data, models, and phase diagrams in multicomponent oxide systems. Springer, New York

Fang Z, Terakura K, Sawada H, Miyazaki T, Solovyev I (1998) Inverse versus normal NiAs structures as high-pressure phases of FeO and MnO. Phys Rev Lett 81:1027–1030

Fei Y (1995) Thermal expansion. In: Ahrens TJ (ed) Mineral physics and crystallography: a handbook of physical constants. AGU Ref Shelf, vol 2. American Geophysical Union, Washington, pp 29–44

Fei Y (1999) Effects of temperature and composition on the bulk modulus of (Mg, Fe)O. Am Miner 84:272–276

Fei Y, Mao HK (1994) In-situ determination of the NiAs phase of FeO at high-pressure and temperature. Science 266:1678–1680

Ferreira LG, Mbaye AA, Zunger A (1988) Chemical and elastic effects on isostructural phase diagrams: the ε–G approach. Phys Rev B 37:10547–10569

Fischer R, Campbell AJ, Shofner GA, Lord OT, Dera P, Prakapenka VB (2011) Equation of state and phase diagram of FeO. Earth Plan Sci Lett 304:496–502

Fjellvag H, Gronvold F, Stolen S, Hauback BC (1996) On the crystallographic and magnetic structures of nearly stoichiometric iron monoxide. J Sol State Chem 124:52–57

Gale JD (1997) GULP-a computer program for the symmetry adapted simulation of solids. JCS Faraday Trans 93:629–637

Ganguly J, Kennedy GC (1974) The energetics of natural solid solution. 1. Mixing of the aluminosilicate end-members. Contrib Miner Petrol 48:137–148

Ganino C, Arndt NT, Chauvel C, Jean A, Athurion C (2013) Melting of carbonate wall rocks and formation of the heterogeneous aureole of the Panzhihua intrusion, China. Geosci Front 4:535–546

Garnero E (2000) Heterogeneity of the lower mantle. Annu Rev Earth Planet Sci 28:509–537

Geiger CA, Newton RC, Kleppa OJ (1987) Enthalpy of mixing of synthetic almandine-grossular and almandine-pyrope garnets from high-temperature solution calorimetry. Geochim Cosmochim Acta 51:1755–1763

Goncharov F, Struzhkin VV, Jacobsen SD (2006) Reduced radiative conductivity of low-spin (Mg, Fe)O in the lower mantle. Science 312:1205–1208

Grønvold F, Stølen S, Tolmach P, Westrum EF (1993) Heat capacities of the wüstites $Fe_{0.9379}O$ and $Fe_{0.9254}O$ at temperatures T from 5 K to 350 K. Thermodynamics of the reaction: xFe(s) + (1/4)Fe$_3$O$_4$(s) = $Fe_{0.7500+x}O$(s) = $Fe_{1-y}O$(s) at T ≈ 850 K, and properties of $Fe_{1-y}O$(s) to T = 1000 K. Thermodynamics of formation of wüstite. J Chem Thermodyn 25:1089–1117

Haider S, Grau-Crespo R, Devey AJ, de Leeuw NH (2012) Cation distribution and mixing thermodynamics in Fe/Ni thiospinels. Geochim Cosmochim Acta 88:275–282

Hasegawa M, Tsukamoto T, Masanori I (2006) Activity of iron oxide in magnesiowürstite in equilibrium with solid metallic iron. Mater Trans 47:854–860

Hill R (1974) Energy-gap variations in semi-conductor alloys. J Phys C Solid State Phys 7:521–526

Hirose K, Lay T (2008) Discovery of post-perovskite and new views on the core–mantle boundary region. Elements 4:183–189

Holland TJB, Powell R (1998) An internally consistent data set for phases of petrological interest. J Metamorph Geol 16:309–343

Irifune T, Shinmei T, McCammon CA, Miyajima N, David C, Rubie DC, Frost DJ (2010) Iron partitioning and density changes of pyrolite in earth's lower mantle. Science 327:193–195

Jacobsen SD, Reichmann HJ, Spetzler HA, Mackwell SJ, Smyth JR, Angel RJ, McCammon CA (2002) Structure and elasticity of single-crystal (Mg, Fe)O and a new method of generating shear waves for gigahertz ultrasonic interferometry. J Geophys Res 107:1–13

Jeanloz R, Ahrens T (1980) Equation of state of FeO and CaO. Geophys J R Astron Soc 62:505–528

Jeanloz R, Knittle E (1989) Density and composition of the lower mantle. Philos Trans R Soc Lond Ser A 328:377–389

Jeanloz R, Lay T (1993) The core–mantle boundary. Sci Am 268:26–33

Kantor I, Dubrovinsky L, McCammon C, Kantor A, Pascarelli S, Aquilanti G, Wilson C, Mattesini M, Ahuja R, Almeida J, Urusov V (2006) Pressure-induced phase transition in $Mg_{0.8}Fe_{0.2}O$ ferropericlase. Phys Chem Miner 33:35–44

Karki BB, Stixrude L, Clark SJ, Warren MC, Ackland GJ, Crain J (1997) Structure and elasticity of MgO at high pressure. Am Miner 82:51–60

Kittel C (2005) Introduction to solid state physics (8th edn). Wiley, New York. ISBN978-0-471-41526-8

Kojitani H, Akaogi M (1994) Calorimetric study of olivine solid solutions in the system Mg_2SiO_4–Fe_2SiO_4. Phys Chem Miner 20:536–540

Kondo T, Ohtani E, Hirao N, Yagi T, Kikegawa T (2004) Phase transitions of (Mg, Fe)O at megabar pressures. Phys Earth Planet Inter 143:201–213

Kubaschewki O, Alcock CB, Spencer RJ (1993) Materials thermochemistry, 6th edn. Pergamon Press, Oxford

Kwong K, Bennet J, Krabbe R, Petty A, Thoms H (2009) Thermodynamic calculations predicting MgO saturated EAF slag for use EAF steel production. In Supplemental proceedings. Materials characterization, computation and modeling. TMS (The Minerals, Melts & Materials Society), vol 2, pp 63–70

Lee C, Yang W, Parr RG (1988) Development of the Colle–Salvetti correlation-energy formula into a functional of the electron density. Phys Rev B 37:785–789

Lee KKM, O'Neill B, Panero WR, Shim SH, Benedetti LR, Jeanloz R (2004) Equations of state of the high-pressure phases of a natural peridotite and implications for the Earth's lower mantle. Earth Planet Sci Lett 223:381–393

Lewis GV, Catlow CRA (1985) Potential models for ionic oxides. J Phys C Solid State Phys 18:1149–1162

Lin JF, Wenk HR, Voltolini M, Speziale S, Shu J, Duffy TS (2009) Deformation of lower-mantle ferropericlase (Mg, Fe)O across the electronic spin transition. Phys Chem Miner 36:585–592

Lin JF, Speziale S, Mao Z, Marquardt H (2013) Effects of the electronic spin transitions of iron in lower mantle minerals: implications for deep mantle geophysics and geochemistry. Rev Geophys 5:244–275

Lyubutin IS, Gavriliuk AG, Frolov KV, Lin JF, Troyan IA (2009) High-spin–low-spin transition in Magnesiowüstite (Mg0.75, Fe0.25)O at high pressures under hydrostatic conditions. JETP Lett 90:617–622

Lyubutin IS, Struzhkin VV, Mironovichc AA, Gavriliuk AG, Naumova PG, Lin J-F, Ovchinnikov SG, Sinogeikin S, Chow P, Xiao Y, Hemley RJ (2013) Quantum critical point and spin fluctuations in lower-mantle ferropericlase. PNAS 110:7142–7147

Mao HK, Shu JF, Fei YW, Hu JZ, Hemley RJ (1996) The wüstite enigma. Phys Earth Planet Inter 96:135–145

McCammon CA, Ringwood AE, Jackson I (1983) Thermodynamics of the system Fe–FeO–MgO at high pressure and temperature and a model for formation of the earth's core. Geophys J R Astron Soc 72:577–595

Meyer A, D'Arcò P, Orlando R, Dovesi R (2009) Andradite-Uvarovite solid solutions. An ab Initio All-Electron Quantum Mechanical

Simulation with the CRYSTAL06 Code. J Phys Chem C 113:14507–14511

Müller T, Baumgartner LP, Foster CT, Bowman JR (2009) Crystal size distribution of periclase in contact metamorphic dolomite marbles from the southern Adamello Massif, Italy. J Petrol 50:451–465

Oganov A, Dorogokupets PI (2003) All-electrons and pseudopotential study of MgO: equation of state, anharmonicity and stability. Phys Rev B 67:224110-1/11

O'Neill HSC, Powneeby MI, McCammon CA (2003) The magnesiowüstite: iron equilibrium and its implications for the activity-composition relations of (Mg, Fe)2SiO4 olivine solid solutions. Contrib Miner Petrol 146:308–325

Ottonello G, Civalleri B, Ganguly J, Vetuschi Zuccolini M, Noel Y (2008) Thermo-physical properties of the a–b–c polymorphs of Mg_2SiO4: an all-electron ab initio study. Phys Chem Miner 36:87–106

Ottonello G, Civalleri B, Ganguly J, Perger WF, Belmonte D, Vetuschi Zuccolini M (2010) Thermo-chemical and thermo-physical properties of the high pressure phase anhydrous $B(Mg_{14}Si_5O_{24})$: an ab initio all-electron investigation. Am Mineral 95:563–573

Pasternak MP, Taylor RD, Jeanloz R, Li X, Nguyen JH, McCammon CA (1997) High pressure collapse of magnetism in $Fe_{0.94}O$: mössbauer spectroscopy beyond 100 GPa. Phys Rev Lett 79:5046–5049

Pavese A, Diella V (2007) Uncertainties on elastic parameters and occupancy factors: How do they affect the accuracy of the calculated Gibbs energy of minerals at (P, T) conditions? The case of 3T-versus 2M1-phengite. Phys Chem Miner 34:637–645

Persson K, Bengtson A, Ceder G, Morgan D (2006) Ab initio study of the composition dependence of the pressure-induced spin transition in the (Mg1x, Fex)O system. Geophys Res Lett 3:L16306

Righter K, Drake MJ, Scott ERD (2006) Compositional relationships between meteorites and terrestrial planets. In: Lauretta D, McSween HY Jr (eds) Meteorites and the early solar system II. University of Arizona Press, Tucson, pp 803–828

Rosenhauer M, Mao HK, Woermann E (1976) Compressibility of magnesiowtistite (Fe0.4Mg0.60) to 264 kbar. Year Book Carnegie Inst Wash 75:513–515

Ruiz-Hernandez SE, Grau-Crespo R, Ruiz-Salvador AR, Nora H, De Leeuw NH (2010) Thermochemistry of strontium incorporation in aragonite from atomistic simulations. Geochim Cosmochim Acta 74:1320–1328

Sanchez JM, Ducastelle F, Gratias D (1984) Generalized cluster description of multicomponent systems. Phys A 128:334–350

Scanavino I, Prencipe M (2013) Ab-initio determination of high-pressure and high-temperature thermoelastic and thermodynamic properties of low-spin (Mg1–xFex)O ferropericlase with x in the range [0.06, 0.59]. Am Miner 98:1270–1278

Scanavino I, Belousov R, Prencipe M (2012) Ab initio quantum-mechanical study of the effects of the inclusion of iron on thermoelastic and thermodynamic properties of periclase (MgO). Phys Chem Miner 39:649–663

Simons B (1980) Composition-lattice parameter relationship of the magnesiowüstite solid solution series. Year Book Carnegie Inst Wash 79:376–380

Smolin A, Schmalzried H (2003) Electrochemically driven solid state reactions in magnesium-wüstite. Phys Chem Phys 5:2248–2252

Speziale S, Milner A, Lee VE, Clark SM, Pasternak MP, Jeanloz R (2005) Iron spin transition in earth's mantle. Proc Natl Acad Sci 102:17918–17922

Sreçec I, Ender A, Woermann E, Gans W, Jacobsson E, Eriksson G, Rosen E (1987) Activity-composition relations of the magnesiowüstite solid solution series in equilibrium with metallic iron in the temperature range 1050–1400 K. Phys Chem Miner 14:492–498

Stølen S, Grande T (2004) Chemical thermodynamics of materials: macroscopic and microscopic aspects. Wiley, England

Stølen S, Gløckner R, Grønvold F, Atake T, Izumisawa S (1996) Heat capacity and thermodynamic properties of nearly stoichiometric wüstite from 13 to 450 K. Am Miner 81:973–981

Taurian OE, Springborg M, Christensen NE (1985) Self-consistent electronic structures of MgO and SrO. Solid State Commun 55:351–355

Valerio G, Catti M, Dovesi R, Orlando R (1995) Ab initio study of antiferromagnetic rutile-type FeF2. Phys Rev B 52:2422–2427

Van der Hilst RD, Widiyantoro S, Engdahl ER (1997) Evidence for deep mantle circulation from global tomography. Nature 386:578–584

Vinograd VL, Winkler B (2010) An efficient cluster expansion method for binary solid solutions: application to the halite-silvite, NaCl–KCl, system. Rev Miner Geochem 71:413–436

Vinograd VL, Brandt F, Rozova K, Klinkenberga M, Refsonc K, Winkler B, Bosbacha D (2013) Solid–aqueous equilibrium in the $BaSO_4$–$RaSO_4$–H_2O system: first-principles calculations and a thermodynamic assessment. Geochim Cosmochim Acta 122:398–417

Wallmach T, Hatton CJ, Droop GTR (1989) Extreme facies of contact metamorphism developed in calc-silicate xenoliths in the Eastern Bushveld complex. Can Miner 27:509–523

Wenzel T, Baumgartner LP, Brügmann GE, Konnikov EG, Kislov EV (2002) Partial melting and assimilation of dolomitic Xenoliths by mafic magma: the Ioko-Dovyren intrusion (North bajkal Region, Russia). J Petrol 43:2049–2074

Wood BJ, Kleppa OJ (1981) Thermochemistry of forsterite-fayalite olivine solutions. Geochim Cosmochim Acta 45:529–553

Wu Z, Cohen RE (2006) More accurate generalized gradient approximation for solids. Phys Rev B 73:235116

Yagi T, Suzuki T, Akimoto S (1985) Static compression of wüstite (Fe0.98O) to 120 GPa. J Geophys Res 90:8784–8788

Yagi T, Fukuoka K, Takei H, Syono Y (1988) Shock compression of wüstite. Geophys Res Lett 15:816–819

Yao YX, Sun Y, Wang HZ, Li YF (2013) Chemical state, site, solid solubility, and magnetism of Fe in the ferropericlase $(Mg_{1-x}Fe_x)O$ produced by ball milling of MgO and Fe. Metall Mater Trans A 44:4551–4557

Yoshiasa A, Sugiyama K, Sakai S, Isobe H, Sakamoto D, Ota K, Arima H, Takei H (2009) Synthesis of single crystal$(Mg_{1-x}Fe_x)_{1-\delta}O$ ($\chi = 0.001$–1.00) solid-solution and electrical conduction mechanism at high temperature and pressure. J Cryst Growth 311:974–977

Zhang J (2000) Effect of defects on the elastic properties of wüstite. Phys Rev Lett 84:507–511

Zhang J, Kostak P (2002) Thermal equation of state of magnesiowüstite $(Mg_{0.6}Fe_{0.4})O$. Phys Earth Plan Int 129:301–311

Zhao CZ, Zhang R, Liu B, Fu DY, Li M, Xiu ZQ, Xie ZL, Zheng YD (2012) A modified simplified coherent potential approximation model of band gap energy of III-V ternary alloys. Sci China Phys Mech Astron 55:400–403